Review   **Open Access**

Photopatterning via photofluidization of azobenzene polymers

Hong Suk Kang[1,2,*] and Shu Yang[1,*]

Abstract

In current photo-based patterning techniques, an image is projected onto a photosensitive material to generate a pattern in the area where the light is focused. Thus, the size, shape, and periodicity of the pattern are determined by the features on the photomask or projected images, and the materials themselves generally do not play an active role in changing the features. In contrast, azobenzene polymers offer a unique type of photopatterning platform, where photoisomerization of the azobenzene groups can induce substantial material movements at the molecular, micro-, and macroscales. Stable surface relief patterns can be generated by exposure to interference light beams. Thus, periodic nano- and microstructures can be fabricated with both two- and three-dimensional spatial control over a large area in a remarkably simple way. Polarized light can be used to guide the flow of solid azobenzene polymers along the direction of light polarization via an unusual solid-to-liquid transition, allowing for the fabrication of complex structures using light. This review summarizes the recent progress in advanced manufacturing using azobenzene polymers. This includes a brief introduction of the intriguing optical behaviors of azobenzene polymers, followed by discussions of the recent developments and successful applications of azobenzene polymers, especially in micro- and nanofabrication.

Keywords: Manufacturings, Photopatterning, Photofluidization, Azobenzene polymers

Introduction

The manufacturing of micro- and nanoscale patterns has broad applications in optics[1], biology[2], and microelectronics[3]. These patterns can be achieved using top-down approaches, such as photolithography[4] and imprinting[5] or bottom-up approaches, such as the growth of nanowires[6] or self-assembly of block copolymers[7]. Laser-based techniques have recently emerged owing to their flexibility for the rapid manufacturing of arbitrary structures with precise control of the laser beam on

Correspondence: Hong Suk Kang (hongsukk@krict.re.kr) or Shu Yang (shuyang@seas.upenn.edu)

[1]Department of Materials Science and Engineering, University of Pennsylvania, 3231 Walnut Street, Philadelphia, PA 19104, USA

[2]Interface Materials and Chemical Engineering Research Center, Korea Research Institute of Chemical Technology (KRICT), 141 Gajeong-ro, Yuseong-gu, Daejeon 34114, Republic of Korea

photoresponsive materials, which comprise macromolecules that undergo physical and chemical changes upon light irradiation at a specific wavelength. These changes lead to large-scale motion or macroscopic movements within the material system[8,9]. Photoresponsive materials have been widely studied in many fields, including photo-optical media[9], photoswitches[10], photomechanical systems[11], micro- and nano-patterning[12], and nonlinear optical media[13,14]. Photoresponsive materials are typically prepared by incorporating photoresponsive chromophores, such as azobenzene[15], stilbene[16], spiropyran[17], spirooxazines[18], and fulgides[19], into the main chain or side chains of the polymer. Photoresponsive materials based on azobenzene and its derivatives are broadly termed azobenzene polymers, and these materials have attracted considerable attention owing to their unique

optical responses[20]. Specifically, azobenzene polymers exhibit photo-isomerization involving molecular structure changes under specific wavelengths, thereby altering the intrinsic physical and chemical properties of the material. The most prominent change is anisotropic fluid flow, in which the polymer chains move in a direction parallel to the polarization direction of the irradiated light[21]. Once the light irradiation is removed, the mobile azobenzene polymers immediately solidify. Thus, photofluidization has been exploited in micro- and nano-patterning[22], nanophotonics[23], electrics and electronics[24], and environmental and energy applications[25]. Nevertheless, the exact mechanism of this unique photofluidic movement remains unclear[10,11,14,21−23].

This review provides a brief overview of azobenzene polymers with a focus on the effects of photofluidic movement. Recent advances in this field are discussed, and a few examples of applications of azobenzene polymers in photonics, micro- and nano-structuring, and surface engineering are presented.

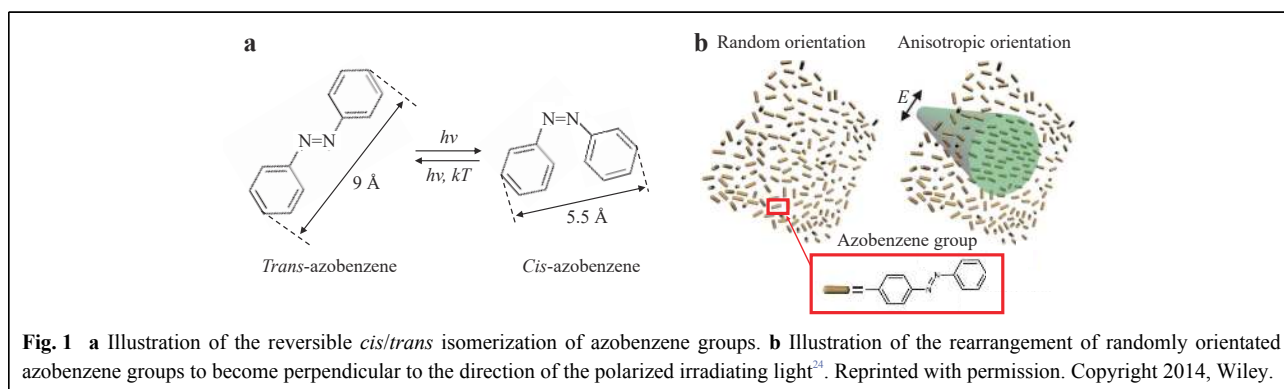## Molecular motion of azobenzene groups in response to light

Azobenzene groups undergo reversible photoisomerization from the stable *trans*-form to the metastable *cis*-form when irradiated with visible or UV light (Fig. 1a). Subsequent irradiation of the *cis*-form by visible light or the use of thermal relaxation leads to isomerization back to the *trans*-form[26]. Notably, the *trans*-form selectively absorbs polarized light along the polarization direction, and the absorbance depends on the angle between the transition moments and the light polarization direction. The *trans*-isomer with transition moments perpendicular to the polarization direction is not activated. In contrast, the *cis*-isomer does not exhibit selective absorbance to the polarization direction of light. Therefore, when exposed to visible or UV light, *trans*- to *cis*- and *cis*- to *trans*- isomerization occur simultaneously in azobenzene molecules owing to the overlap in their optical absorption spectra[27]. Combining the polarization-selective *trans*- to *cis*- isomerization with the unselective *cis*- to *trans*- reversible isomerization, the azobenzene groups will gradually reorient to a plane orthogonal to the polarization direction, which is known as photo-induced alignment (Weigert effect), as shown in Fig. 1b[28].

Isomerization involves substantial changes in the geometric size and dipole moment of the molecules. For example, the distances between the *para*-carbons in *trans*- and *cis*-azobenzene are 9 and 5.5 Å (Fig. 1a)[26,29], respectively, while the dipole moments are 0 and 3.1 D, respectively[30]. At the molecular scale, these differences are significant. The molecular motion resulting from the gradual increase in the dichroic ratio (*i.e.,* the ratio of the absorbance in the parallel direction to that in the perpendicular direction)[31] leads to rearrangement of the randomly arranged groups within the polymer matrix such that they become perpendicular to the polarization direction of the light[24]. This can be attributed to the fact that azobenzene groups preferentially absorb polarized light in the parallel direction; as the groups rearrange in the parallel direction, those perpendicular to the polarization direction begin to accumulate (Fig. 1b)[24].

Photofluidic movement of azobenzene polymers

Pseudo-stilbene azobenzene polymers are characterized by swapped electron-donating and electron-withdrawing groups within the azobenzene ring. This leads to an overlap in the ranges of wavelengths that are absorbed by the *trans*- and *cis*- isomers[32]. Therefore, *trans*- to *cis*- isomerization and *cis*- to *trans*- isomerization can occur simultaneously, resulting in continuous *trans-cis-trans* isomerization cycling during irradiation. These azobenzene polymers liquefy and soften owing to the vibrations caused by cyclic isomerization. This mechanism is similar to how heat energy causes rapid and random vibrations in solid-state

Fig. 1 **a** Illustration of the reversible *cis/trans* isomerization of azobenzene groups. **b** Illustration of the rearrangement of randomly orientated azobenzene groups to become perpendicular to the direction of the polarized irradiating light[24]. Reprinted with permission. Copyright 2014, Wiley.

polymers, which decreases the long-range order and structural symmetry to ultimately liquefy the solid-state polymer[33]. Several models have been proposed to describe this phenomenon, including a thermal model[34], pressure gradient force model[35], mean-field model[36], optical field gradient force model[37,38], and asymmetric diffusion model[39,40]. However, none of these models can completely explain the various liquefying phenomena, particularly those related to the large increase in free volume due to the *cis*- and *trans*- isomer size difference (Fig. 1a) and the rapidly repeating isomerization (on the order of picoseconds) (Fig. 2a)[41]. Light irradiation leads to the disappearance of the elastic region in the load–penetration curves of azobenzene polymer films in the absence of irradiation (Fig. 2b)[21], while angular azobenzene polymer pillars become rounded[42]. Both changes demonstrate that azobenzene polymers fluidize under light irradiation (Fig. 2c). We note that this fluidization differs from liquefaction due to heating, as photofluidization occurs near room temperature, which is below the glass transition

Fig. 2 a Rapid repeated isomerization of azobenzene rings (on the order of picoseconds)[41]. Reprinted with permission. Copyright 1998, Elsevier. **b** Load–penetration curves of an azobenzene polymer film before (left) and during (right) light irradiation[21]. Reprinted with permission. Copyright 2005, Springer Nature. **c** Scanning electron microscopy (SEM) images of an angular azobenzene polymer pillar before (left) and after (right) light irradiation[42]. Reprinted with permission. Copyright 2013, Wiley.

temperature (T_g) of the polymer[43]. Photofluidization is based on the bulk isomerization of azobenzene groups; thus, it is often referred to as athermal photofluidization[43].

Fig. 3 summarizes the most widely used azobenzene-containing materials that exhibit the abovementioned photofluidic behaviors. Among them, azobenzene polymers are the most popular materials[23,44–50]; common examples include those based on amorphous polymeric backbones, such as poly(disperse orange 3) (PDO 3)[51] and poly(disperse red 1 methacrylate) (pDR1m) (Fig. 3a)[44]. Novel azobenzene-containing materials have been developed to extend the range of photofluidization, impart new functions, and widen their applications, including (i) azobenzene molecular glasses (Fig. 3b)[52], (ii) a supramolecular approach in which the pendent groups of azobenzene molecules are non-covalently attached to an inorganic precursor (Fig. 3c)[53], and (iii) grafting of azobenzene onto protein-based materials (i.e., azobenzene-functionalized native protein) (Fig. 3d)[54].

Unlike typical heat-induced fluidization, the photofluidic movement of azobenzene polymers is characterized by movement parallel to the light polarization direction (Fig. 4a). For example, an azobenzene polymer film marked with the letter 'X' and subjected to irradiation under linearly polarized light would begin to flow parallel to the polarization direction. Thus, only the sections of the 'X' mark perpendicular to the polarization direction would be filled (Fig. 4a)[21]. This is the most prominent characteristic of the photofluidic movement of azobenzene polymers, and it can be used to control the movement of azobenzene polymers based on the polarization direction. For example, the irradiation of azobenzene polymer pillars with light polarized in various linear or circular directions allows for control over the direction and form of the azobenzene polymer movement (Fig. 4b)[24]. This unique fluidization phenomenon can be attributed to the rapid *trans*- to *cis*- isomerization, which introduces a large free volume in the polymer[41] (Fig. 1a and Fig. 2a) and an anisotropic arrangement of the azobenzene groups only in the direction parallel to the polarized light[21] (Fig. 1b).

As azobenzene polymers undergo an immediate phase transition upon light irradiation, both the magnitude and duration of their movement can be readily controlled by adjusting the light irradiation time and intensity. As shown in Fig. 4c, azobenzene polymer micropillars with a circular cross-section (2 μm in diameter) become ellipsoidal when exposed to linearly polarized light in a specific direction; the aspect ratio of the ellipsoidal cross-section continues to increase with the increase in irradiation time. The fluidization movement speed also increases with increasing

	A	B	X
Tr-AZ-Cl	CH_3	H	Cl
Tr-AZ-CN	CH_3	H	CN
Tr-AZ-NT	CH_3	H	NO_2
Tr-35AZ-Cl	CH_2CH_3	CH_3	Cl
Tr-35AZ-CN	CH_2CH_3	CH_3	CN
Tr-35AZ-NT	CH_2CH_3	CH_3	NO_2
Tr-H35AZ-Cl	CH_2CH_2OH	CH_3	Cl
Tr-H35AZ-CN	CH_2CH_2OH	CH_3	CN
Tr-H35AZ-NT	CH_2CH_2OH	CH_3	NO_2

	M_W of dendrimer	Dendrimer diameter (nm)	Number of end units	M_W of complex
G3-EO	7800	3.7	16	13000
G5-EO	33000	8.0	64	54000
G7-EO	131000	13.7	256	216000
G9-EO	528000	21.4	1024	868000

Fig. 3 Representative examples of materials exhibiting photofluidic movement. **a** Structures of typical azobenzene polymers (PDO 3 and pDR1m). **b** Star-shaped azobenzene molecular glasses. Adapted from[52] Copyright 2011, ACS Publications. **c** Supramolecular approach incorporating azobenzene molecules into an inorganic precursor[53]. Reprinted with permission. Copyright 2015, ACS. **d** Chemical structure and molecular weight of an azobenzene-functionalized native protein[54]. Reprinted with permission. Copyright 2014, ACS.

Fig. 4 **a** Azobenzene polymer marked with the letter 'X' and irradiated with polarization-controlled light. The characteristic of movement parallel to the polarization direction of the light leads to the filling of only Canal 1[21]. Reprinted with permission. Copyright 2005, Springer Nature. **b** SEM images of a square azobenzene polymer pillar irradiated by polarization-controlled light to achieve deformation parallel to the polarization direction of the light[24]. Reprinted with permission. Copyright 2014, Wiley. **c** SEM images of shape changes under varying light irradiation times. **d** Distance of the azobenzene polymer movement under varying light irradiation times and intensities.

irradiation intensity (Fig. 4d).

Micro/nano-structuring and recent applications

This section presents applications of the photofluidic phenomena in both fundamental and technologically oriented studies considering the general rules governing the macroscopic photofluidic movement of azobenzene polymers.

Surface relief gratings on azobenzene polymer films

The irradiation of a thin azobenzene polymer film (typically less than 1 μm thick) with a sinusoidal intensity light pattern leads to the formation of sinusoidally modulated surface relief gratings (SRGs) (Fig. 5a)[42,55]. SRGs with large modulation amplitudes are unique to azobenzene polymer systems. This process differs from other conventional light-based micro- and nanopatterning techniques, such as laser ablation and chemical etching.

Specifically, light-induced SRG formation is a facile one-step procedure, and the modulation amplitude can be precisely controlled by adjusting the irradiation time and polarization states of the irradiating beams. SRGs can be formed at low light intensities (several mW·cm⁻²), which indicates that they are not formed by ablative or destructive processes. Instead, SRGs are known to result from the fluidic movement of azobenzene polymers owing to their high sensitivity to the polarization distribution of the interference light[51,56−58]. The spatial distribution of the polarization state along the grating vector of interference light is presented in Fig. 5b[56], while the topological evolution owing to various types of polarization combinations can be visualized using atomic force microscopy (AFM), as shown in Fig. 5c[56]. The surface relief maxima and minima of the interference pattern are clearly observed at positions with vertically (↕) and horizontally (↔) oscillating polarizations, respectively.
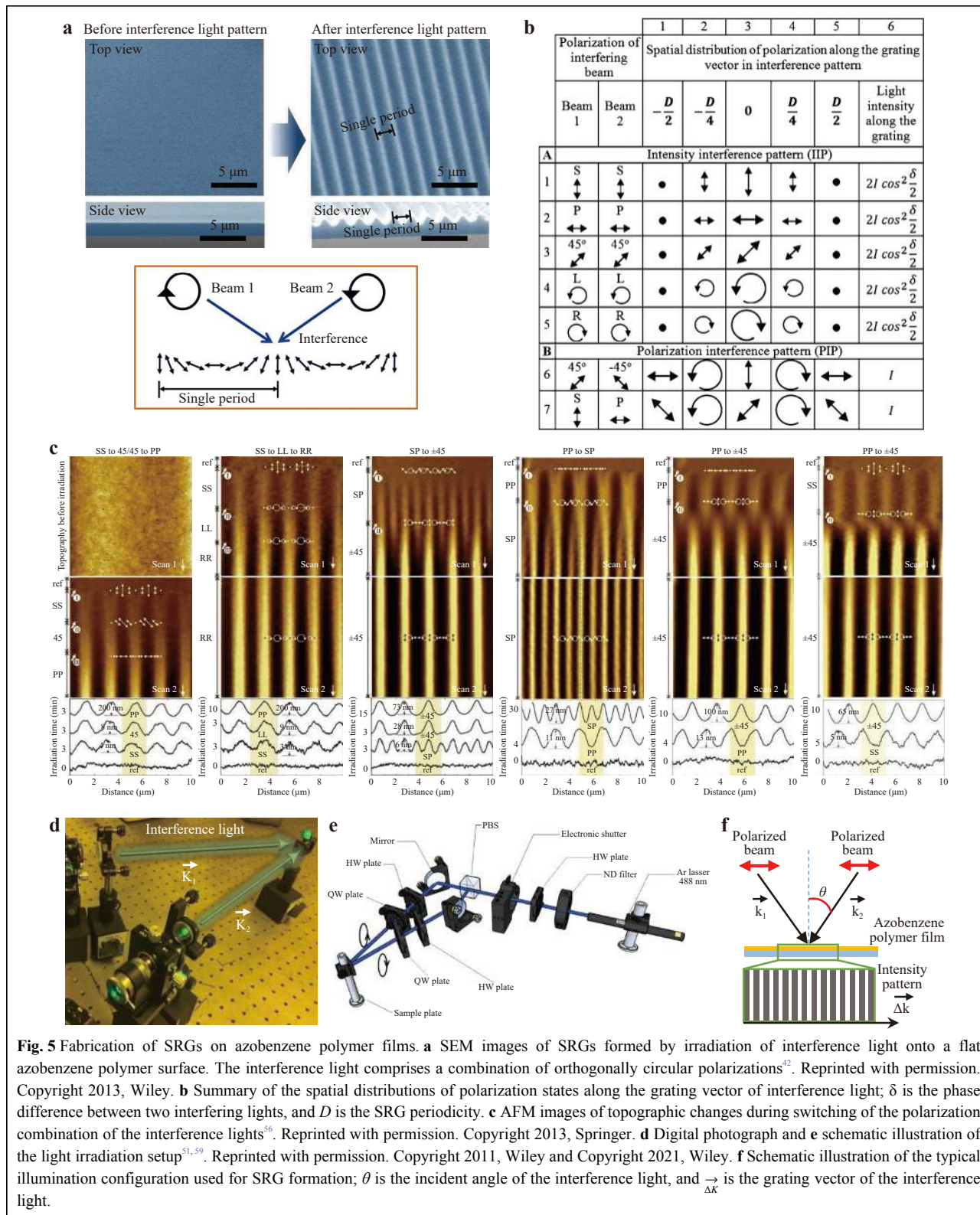
Fig. 5 Fabrication of SRGs on azobenzene polymer films. a SEM images of SRGs formed by irradiation of interference light onto a flat azobenzene polymer surface. The interference light comprises a combination of orthogonally circular polarizations[42]. Reprinted with permission. Copyright 2013, Wiley. **b** Summary of the spatial distributions of polarization states along the grating vector of interference light; δ is the phase difference between two interfering lights, and *D* is the SRG periodicity. **c** AFM images of topographic changes during switching of the polarization combination of the interference lights[56]. Reprinted with permission. Copyright 2013, Springer. **d** Digital photograph and **e** schematic illustration of the light irradiation setup[51, 59]. Reprinted with permission. Copyright 2011, Wiley and Copyright 2021, Wiley. **f** Schematic illustration of the typical illumination configuration used for SRG formation; θ is the incident angle of the interference light, and $\overrightarrow{\Delta K}$ is the grating vector of the interference light.

This confirms that the formation of SRGs occurs during the polarization movement of azobenzene polymers.

A typical experimental setup for the preparation of SRGs is presented in Fig. 5d and 5e[51,59]. Laser beams with wavelengths of either 488 or 532 nm are spatially filtered, collimated, and split into two beams of equal intensity. The

two beams are reflected by mirrors and recombined to form an interference pattern at the recording medium plane. The two interfering lights independently pass through half-wave ($\lambda/2$) plates to control the linear polarization state of the recording beams. Interference light comprising different polarization states can be achieved by controlling these half-wave plates, while circularly polarized beams can be obtained by replacing the half-wave plates with quarter-wave ($\lambda/4$) plates. SRGs can be formed by exposing an azobenzene polymer film to an interference pattern of appropriately polarized beams, where the angle (θ) between the interfering beams can be adjusted to obtain the desired grating periodicity (D, see Fig. 5f)[60] according to Bragg's law:
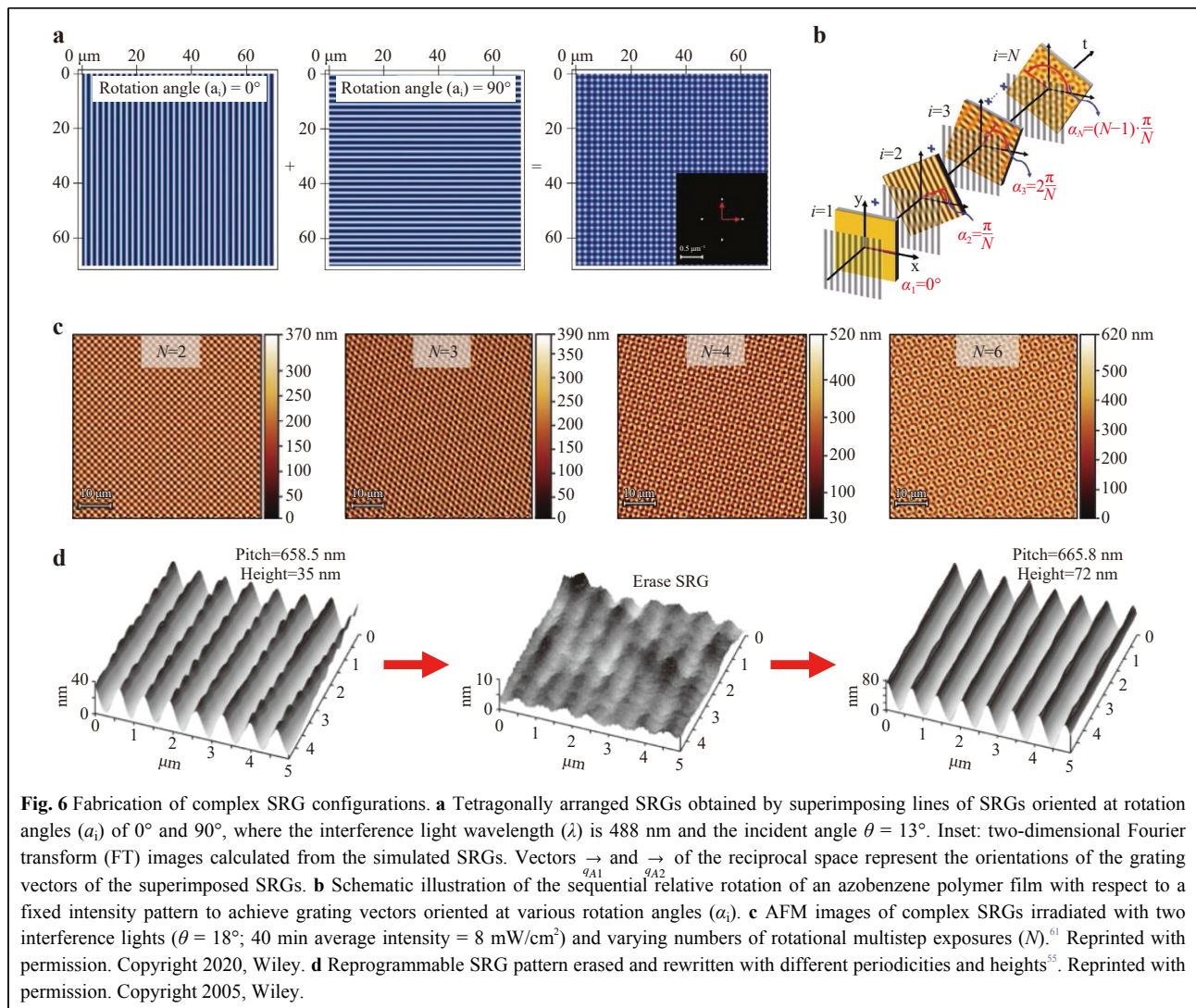
$$D = \frac{2}{\sin(\theta/2)} \qquad (1)$$

Most studies use recording beam intensities of 5–100 mW·cm^{-2} to avoid sample heating and spurious photothermal effects[42,51].

SRGs with tetragonal, hexagonal, or even more complex symmetries can be generated based on two or multiple sequential inscriptions of simple SRGs in different directions[61,62]. For example, tetragonally arranged SRGs can be obtained by superimposing lines of SRGs by rotating the sample 90° between two sequential exposure steps under a fixed interference light (Fig. 6a). Increasing the number of sequential exposures and controlling the sample rotation angle at each stage allows for the design of rotationally symmetric complex surface textures over large areas (Fig. 6b, c). Furthermore, amplitudes of several hundreds of nanometers and periodicities ranging from hundreds of nanometers to several micrometers can be achieved[61].

The formation of SRGs offers the potential for cost-

Fig. 6 Fabrication of complex SRG configurations. **a** Tetragonally arranged SRGs obtained by superimposing lines of SRGs oriented at rotation angles (a_i) of 0° and 90°, where the interference light wavelength (λ) is 488 nm and the incident angle $\theta = 13°$. Inset: two-dimensional Fourier transform (FT) images calculated from the simulated SRGs. Vectors $\overrightarrow{q_{A1}}$ and $\overrightarrow{q_{A2}}$ of the reciprocal space represent the orientations of the grating vectors of the superimposed SRGs. **b** Schematic illustration of the sequential relative rotation of an azobenzene polymer film with respect to a fixed intensity pattern to achieve grating vectors oriented at various rotation angles (a_i). **c** AFM images of complex SRGs irradiated with two interference lights ($\theta = 18°$; 40 min average intensity = 8 mW/cm^2) and varying numbers of rotational multistep exposures (N).[61] Reprinted with permission. Copyright 2020, Wiley. **d** Reprogrammable SRG pattern erased and rewritten with different periodicities and heights[55]. Reprinted with permission. Copyright 2005, Wiley.

effective all-optically driven surface structuration. The periodicity of SRGs can be controlled by adjusting the irradiation wavelength and incidence angle of the collimated beams (Fig. 5f)[59]. Thus, the inscribed surface modulation may be tuned. In addition, SRG patterns can be reprogrammed by erasing and rewriting the SRG with another structure, regardless of the degree of geometric complexity (Fig. 6d)[21,55,59,62]. This is possible owing to the reversible nature of the photofluidic motion of the azobenzene polymers[63]. This advantage is particularly relevant in the development of all-reversible optical-patterned surfaces, where the removal of inscribed superficial structures under irradiation with circularly polarized or unpolarized light is required. Thus, unwanted patterns can be selectively erased by simply shining a beam with a spatially structured intensity profile onto the film surface, and a new grating vector can be generated within specified areas of the film, e.g., by using a transmission mask[59].

Fabrication and applications of surface relief gratings

The periodic structures of SRGs can be patterned and reconfigured at will over areas of a few square centimeters with amplitudes up to 1 μm and periods ranging from hundreds of nanometers to several micrometers[59]. The patterned surfaces maintain their quality for at least several years under ordinary storage conditions[64]. These features of azobenzene polymers offer significant potential for use in micro- and nanopatterning[23,59,65−67] as well as for the fabrication of various photonic elements, such as diffraction gratings[35,68−70], microlens arrays[71], photonic crystals[72], distributed feedback lasers (DFB)[55], perfect absorbers[73], plasmonic nanostructures[74], and recently proposed optical metasurfaces and metamaterials[59].
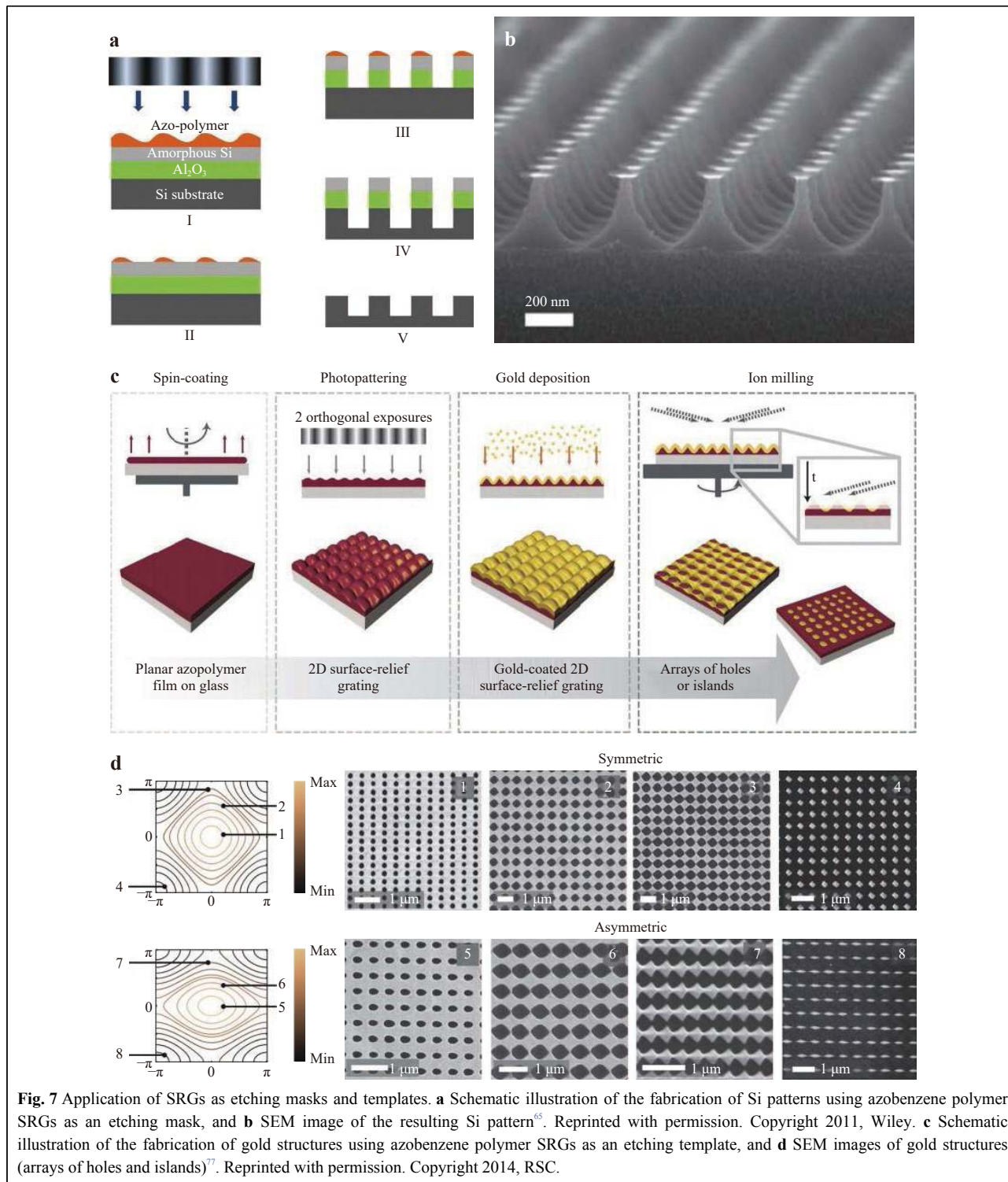
Similar to photoresists, azobenzene polymers can also be used to make etching masks to create patterns, e.g., on a Si wafer via reactive ion etching (RIE) (Fig. 7a, b)[65]. Because SRGs are produced under ambient room light, they offer better tolerance to overexposure than traditional photoresists. The etching contrast of the Si wafer versus the photoresist can be increased by introducing a 5 nm-thick layer of Al_2O_3 and a 20 nm-thick amorphous Si layer beneath the azobenzene polymer layer. The Al_2O_3 layer acts as a hard mask, and the amorphous Si ensures tight adhesion between the azobenzene polymer layer and the substrate. Fig. 7a shows a multi-layered approach for pattern transfer, where the azobenzene polymer mask pattern is first transferred onto the amorphous Si via RIE, followed by wet etching of the Al_2O_3 layer and dry etching of the underlying Si substrate. An example of the resulting

silicon nanocones is shown in Fig. 7b, which are promising for applications such as self-cleaning superhydrophobic or superoleophobic surfaces[75] and anti-reflective coatings[76].

Azobenzene polymer SRGs can also be used as etching templates (Fig. 7c, d)[77]. A thin gold layer is electron-beam deposited on tetragonally aligned SRGs. Subsequently, the crests of the gold-coated grating are etched using ion-beam milling to form plasmonic arrays. The symmetry of the resulting structure can be controlled by adjusting the irradiation time of the first and second SRG inscriptions (Fig. 7d). The size of the structures is determined by the ion-beam milling time: a short milling time produces dielectric openings in the gold film, and a long milling time leads to the formation of discrete nano-sized gold islands.
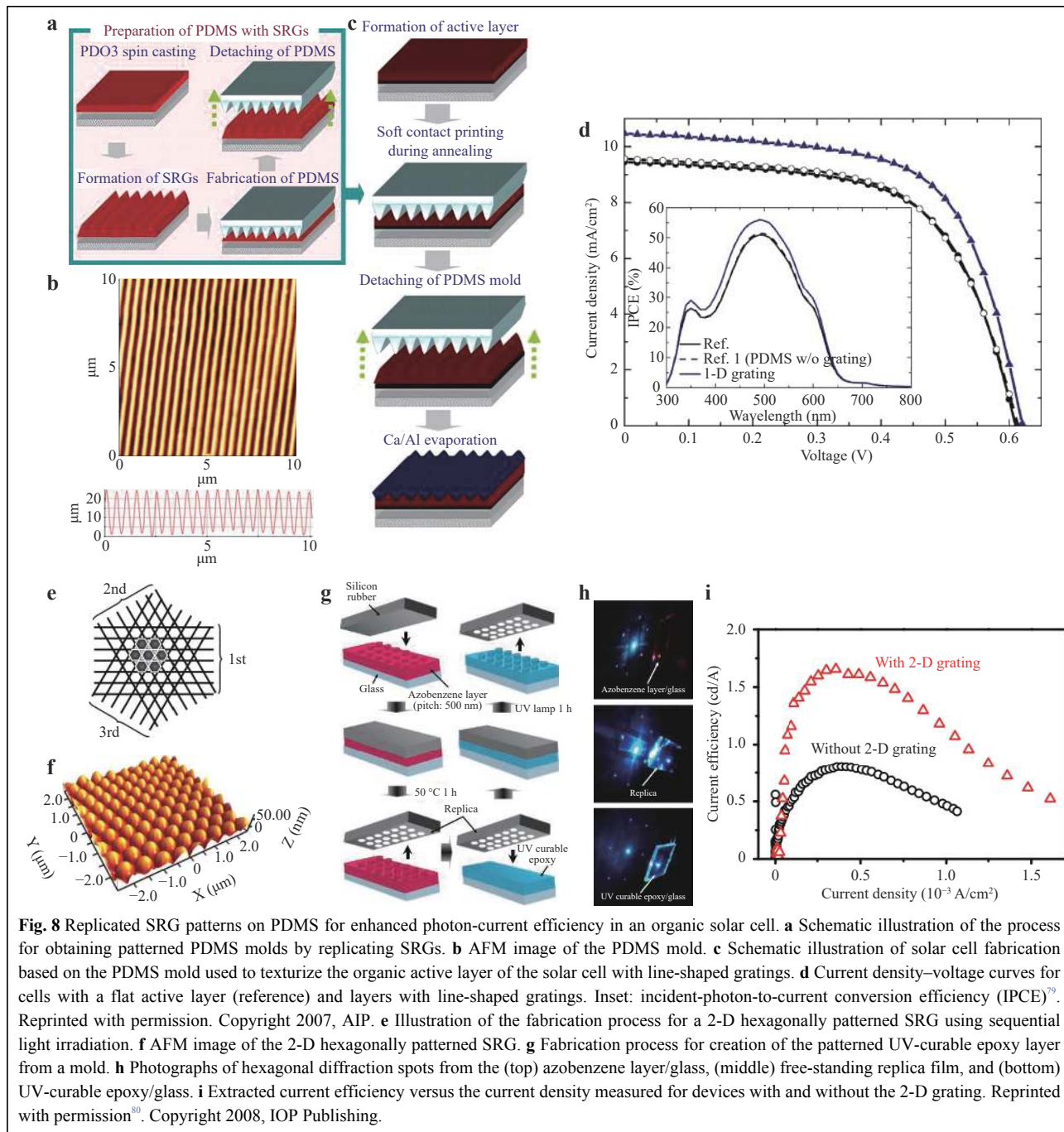
Direct applications of azobenzene polymer SGRs in optical devices can be difficult, because problems such as photo-bleaching or undesired photofluidic movement can occur during device operation. Furthermore, azobenzene polymers are typically opaque in the ultraviolet (UV)/ visible spectral regions. These limitations can be overcome by transferring textured SRGs onto an elastomeric polymer such as poly(dimethylsiloxane) (PDMS) via replica molding[78]. PDMS-based replica molding of line- and dome-array SRGs has been reported to enhance the performance of photovoltaic devices (Figs. 8a−d)[79]. Fig. 8a shows a technique for fabricating such an organic photovoltaic cell. An azobenzene polymer-based SRG is used as the master to create a PDMS stamp; an AFM image of the stamp is shown in Fig. 8b. Fig. 8c shows the fabrication process, which includes soft-contact imprinting of the SRG onto the active layer and subsequent thermal evaporation of calcium and aluminum onto the patterned surface. The absorption efficiency of photons propagating in the textured active layer is enhanced by imprinting the SRG texture onto the active layer, and the performance of the organic photovoltaic cells is improved owing to the substantial diffraction of incident sunlight by the textured surface (Fig. 8d). According to the literature, such structuring can increase the cell efficiency by approximately 15%[79].

Similarly, the performance of a solid-state DFB laser[55], the light extraction efficiency of light emitting diodes (LED)[80], and other optoelectronic devices can be improved using SRG textures[81,82]. For example, Figs. 8e−g demonstrate that a simple 2-D hexagonally patterned SRG structure can be used to improve the performance of OLEDs[80]. Fig. 8e illustrates the fabrication of a hexagonally patterned SRG structure using sequential light irradiation. The AFM image in Fig. 8f confirms the successful formation of a hexagonal nanopattern with a pitch of 500 nm and a depth of 50 nm. For photovoltaic

Fig. 7 Application of SRGs as etching masks and templates. **a** Schematic illustration of the fabrication of Si patterns using azobenzene polymer SRGs as an etching mask, and **b** SEM image of the resulting Si pattern[65]. Reprinted with permission. Copyright 2011, Wiley. **c** Schematic illustration of the fabrication of gold structures using azobenzene polymer SRGs as an etching template, and **d** SEM images of gold structures (arrays of holes and islands)[77]. Reprinted with permission. Copyright 2014, RSC.

applications, the patterned azobenzene polymer film is replicated to create a master made from UV-transparent silicon rubber, which is further replicated with UV-curable epoxy onto the glass substrate, as shown in Fig. 8g. In 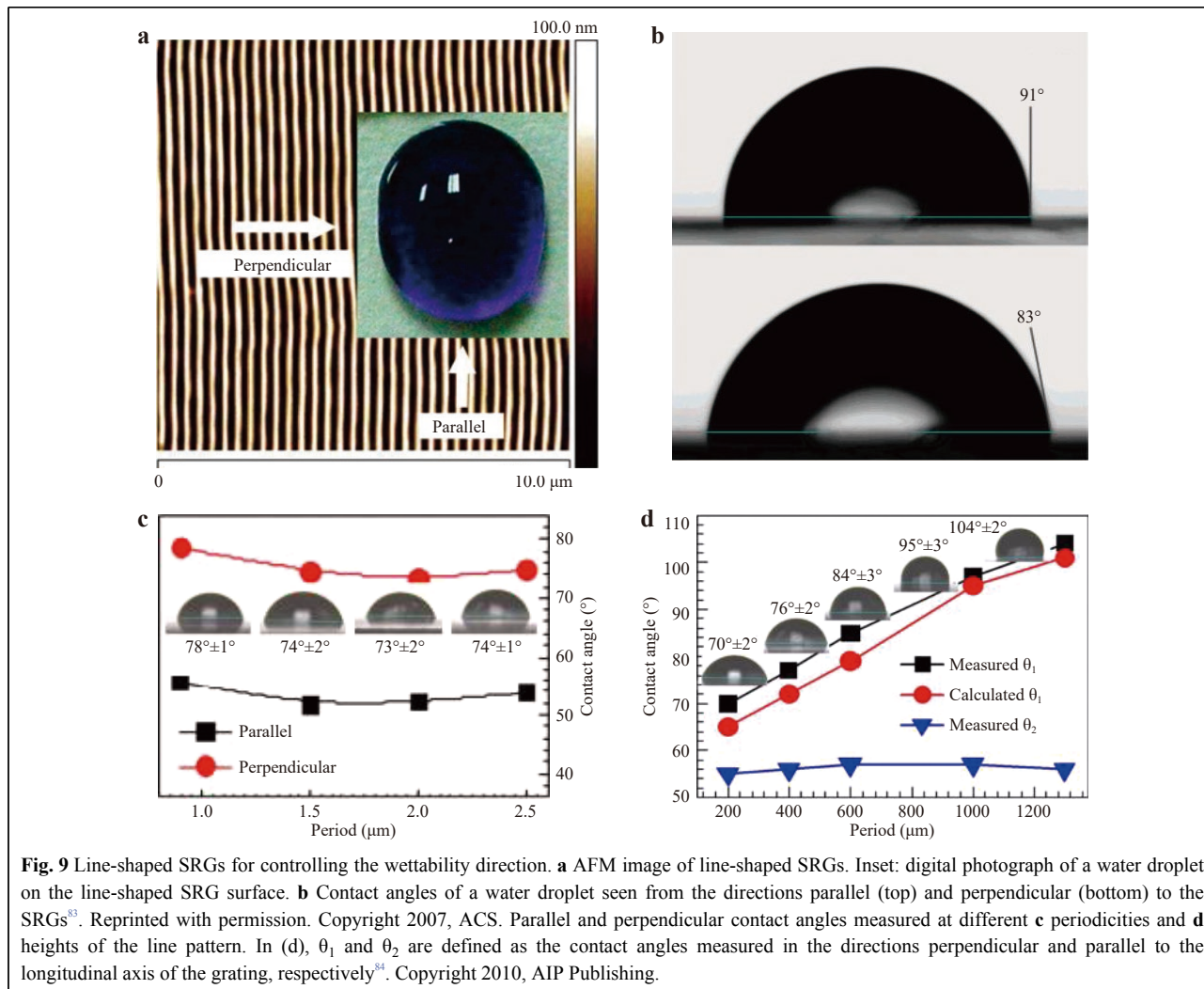Fig. 8h, hexagonal diffraction light patterns can be clearly observed in the azobenzene polymer/glass, free-standing silicon rubber, and UV-cured epoxy/glass during irradiation with a He–Cd laser beam (325 nm), indicating a high fidelity of replication. Finally, the extracted current efficiency of an electro-luminescent (EL) device with

Fig. 8 Replicated SRG patterns on PDMS for enhanced photon-current efficiency in an organic solar cell. **a** Schematic illustration of the process for obtaining patterned PDMS molds by replicating SRGs. **b** AFM image of the PDMS mold. **c** Schematic illustration of solar cell fabrication based on the PDMS mold used to texturize the organic active layer of the solar cell with line-shaped gratings. **d** Current density–voltage curves for cells with a flat active layer (reference) and layers with line-shaped gratings. Inset: incident-photon-to-current conversion efficiency (IPCE)[79]. Reprinted with permission. Copyright 2007, AIP. **e** Illustration of the fabrication process for a 2-D hexagonally patterned SRG using sequential light irradiation. **f** AFM image of the 2-D hexagonally patterned SRG. **g** Fabrication process for creation of the patterned UV-curable epoxy layer from a mold. **h** Photographs of hexagonal diffraction spots from the (top) azobenzene layer/glass, (middle) free-standing replica film, and (bottom) UV-curable epoxy/glass. **i** Extracted current efficiency versus the current density measured for devices with and without the 2-D grating. Reprinted with permission[80]. Copyright 2008, IOP Publishing.

hexagonal patterns is measured and compared with that of an EL device without the 2-D grating, as shown in Fig. 8i. The EL device with the patterned SRG exhibits an extracted current efficiency that is almost twice that of the non-patterned device. This is because the 2-D grating modifies the emitted light through Bragg diffraction into free space instead of trapping it in substrate-guided modes.

Line-shaped SRGs exhibit structural anisotropy, which leads to anisotropic surface properties such as wettability
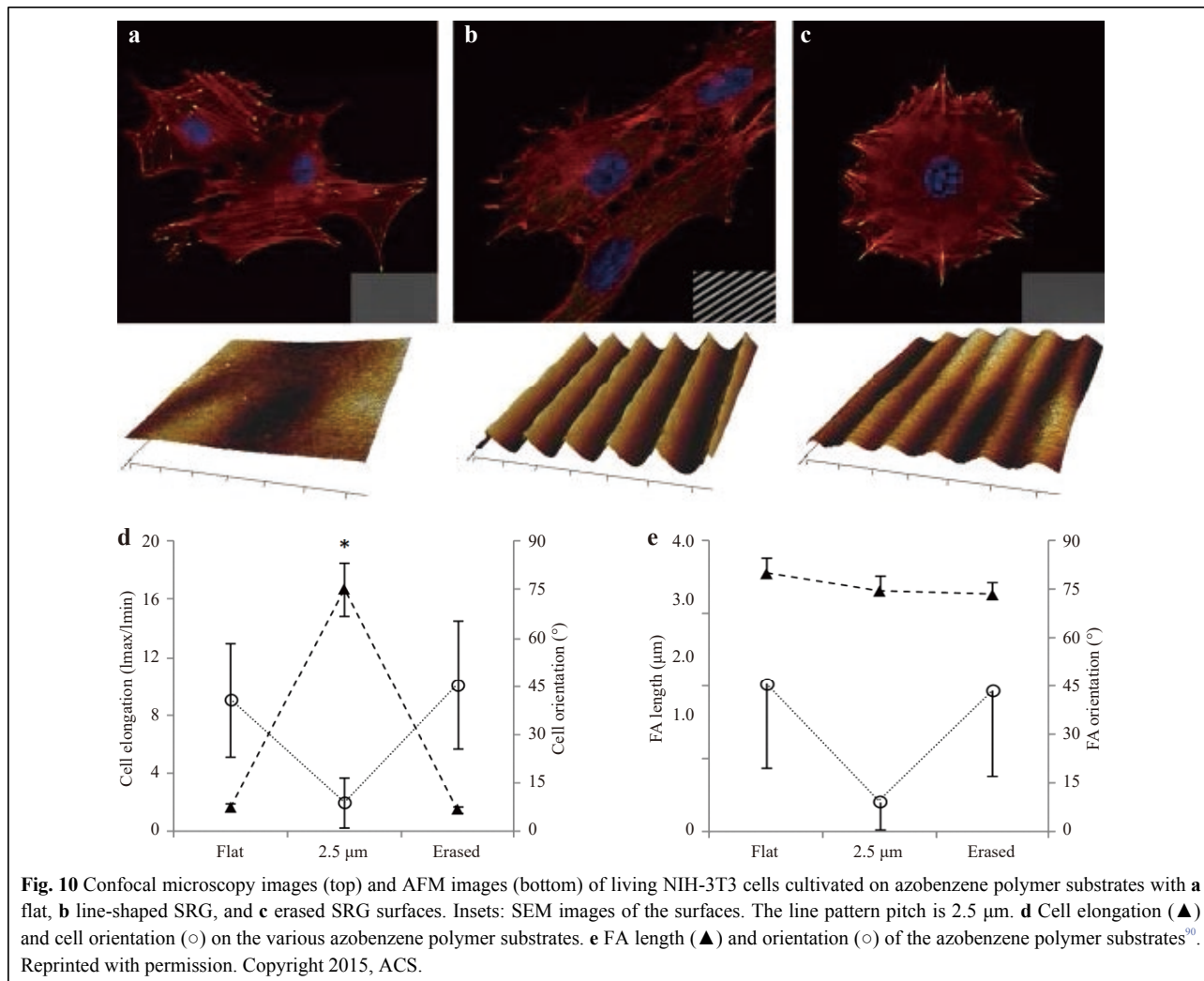
and adhesion (Fig. 9)[83,84]. These properties are highly dependent on the spatial configuration of the superficial roughness. As shown in Fig. 9a, water droplets propagate parallel to the direction of the textured surface owing to the asymmetric elongation of the liquid contact line. Hence, the deposition of a liquid droplet on such an anisotropic surface results in asymmetric elongation of the liquid contact line, which is quantified by the anisotropy in the liquid contact angles measured along different directions of

Fig. 9 Line-shaped SRGs for controlling the wettability direction. **a** AFM image of line-shaped SRGs. Inset: digital photograph of a water droplet on the line-shaped SRG surface. **b** Contact angles of a water droplet seen from the directions parallel (top) and perpendicular (bottom) to the SRGs[83]. Reprinted with permission. Copyright 2007, ACS. Parallel and perpendicular contact angles measured at different **c** periodicities and **d** heights of the line pattern. In (d), θ_1 and θ_2 are defined as the contact angles measured in the directions perpendicular and parallel to the longitudinal axis of the grating, respectively[84]. Copyright 2010, AIP Publishing.

the substrate. Fig. 9b shows the side view of the droplet seen from the directions parallel (top) and perpendicular (bottom) to the SRG texture. D. Wu et al. investigated wetting anisotropy and its relation to the periodicity and height of the pattern (Fig. 9c, d)[84]. In that study, no obvious differences were observed in the anisotropic wetting behavior with varying the periodicity of the pattern from 0.9 to 2.5 μm. Interestingly, the increase in the pattern height resulted in an increase in the water contact angle in the perpendicular direction, but no significant change was observed in the parallel direction. It is notable that the height and periodicity of SRGs prepared from azobenzene polymers can be easily tuned by varying the irradiation parameters (e.g., the incident angle, light irradiation time, or light intensity)[84–86], which is extremely difficult to achieve using other fabrication techniques[87,88].

Line-shaped SRGs can also be used in tissue engineering as extracellular matrices (ECM) to modulate living cells[89,90]; in ECM, the cell attachment, spreading, and differentiation are highly dependent on the surface topography[91]. The mass production potential of controlled large-scale micro-textured SRGs is particularly attractive for investigating cell responses to dynamically varying surface textures in response to external stimuli. The interactions between living cells and a flat surface (Fig. 10a), a line-shaped SRG surface (Fig. 10b), and an optically erased SRG surface (Fig. 10c) are examined using confocal microscopy, and the cells are elongated and reoriented on the line-shaped SRG surface. Notably, cells grown on the pristine flat substrate appear similar to those grown on the optically erased azobenzene polymer substrate, showing random orientations with a broad distribution. The quantification of the cell elongation and orientation is shown in Fig. 10d. The cells have the largest elongation but smallest orientation on the 2.5 μm SRG. The cells are presumably aligned parallel to the direction of the grating

Fig. 10 Confocal microscopy images (top) and AFM images (bottom) of living NIH-3T3 cells cultivated on azobenzene polymer substrates with **a** flat, **b** line-shaped SRG, and **c** erased SRG surfaces. Insets: SEM images of the surfaces. The line pattern pitch is 2.5 μm. **d** Cell elongation (▲) and cell orientation (○) on the various azobenzene polymer substrates. **e** FA length (▲) and orientation (○) of the azobenzene polymer substrates[90]. Reprinted with permission. Copyright 2015, ACS.

with a narrow distribution. The focal adhesion (FA) length remains almost unchanged during the writing/erasing cycles, whereas the FA orientation is influenced by the surface topography, showing parallel FAs on the SRGs (Fig. 10e). Therefore, by writing and rewriting SRGs from azobenzene polymers, the cell alignment on the surface can be fine-tuned accordingly.

Three-dimensional (3D) SRG inscriptions can be used to produce complex hierarchical structures. For example, we previously demonstrated a generic strategy for the fabrication of hierarchical structures via 3D controlled photoengraving of SRGs on azobenzene polymers[59] by exercising additional degrees of control over the light irradiation vectors and surface morphology (*i.e.,* replacing flat surfaces with 3D scaffolds). By projecting different types of interference laser beams, which generate distinct types of SRGs (the secondary structures), onto different facets of a microstructure (the primary structure) fabricated from azobenzene polymers, we could independently

inscribe or erase metasurfaces onto and from individual facets of 3D monoliths with arbitrary shapes and dimensions in a high-throughput fashion (over a few cm² at a time, Fig. 11a). This prospective 3D photoengraving strategy offers significant advantages over other strategies. Specifically, it allows for the deterministic inscription of distinct micro- and nanotextures with modulated heights (e.g., lines, domes, and complex quasi-textures) on every facet of the parent surface. This level of deterministic control over the morphology allows for the preparation of increasingly precise and complex hierarchical architectures. In addition, this strategy remains relatively simple and easy to access, despite offering a high degree of control and flexibility. This is due to the elimination of the wet etching and mechanical contact steps, the capability for large-area fabrication (approximately several square centimeters at a time), and the minimal incidence of defects. As shown in Figs. 11b−d, the 3D photoengraving process is applied to a square array of PDO 3 micropillars
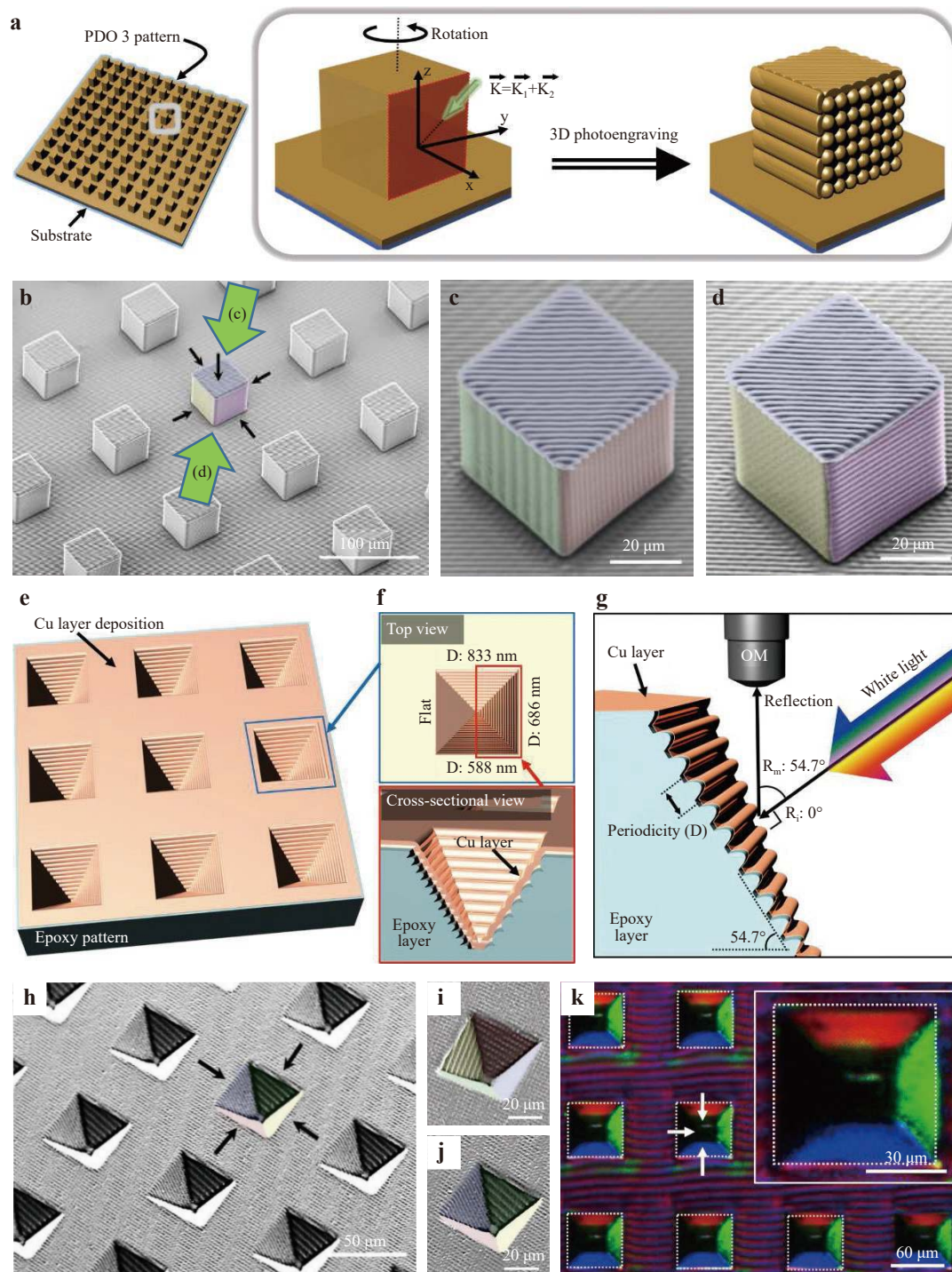
Fig. 11 a Schematic illustration of the 3D photoengraving of a multifaceted micropillar array. **b** SEM images of the hierarchical structures created by 3D photoengraving, comprising primary structures inscribed with various secondary structures of different grating vectors and dimensionalities. **c** and **d** High-magnification views of a single micropillar viewed in opposite directions (viewing directions are marked in **b**). **e−f** Multiplexing metasurface-based color filter with three different pixelated diffraction colors integrated into individual pyramidal multifaceted arrays. The three engraved facets have grating periodicities (*D*) of 588, 686, and 833 nm. **g** Optical setup to observe the reflected colors. **h−j** SEM images of the diverse metasurfaces inscribed on inverse pyramidal arrays. **k** Optical micrographs of the illuminated multiplexing structure-color filter exhibiting red, green, and blue colors when the filter is illuminated with multiple white light. White arrows: direction of the white light illumination. Inset: high-magnification optical micrographs. Reprinted with permission[59]. Copyright 2021, Wiley.

(height = 40 μm, aspect ratio (height/width) = 1, spacing = 100 μm), achieving heterogeneous integration of different types of micro- and nanotextured surfaces with different grating vectors and dimensionalities on each single pillar. This outcome is difficult to achieve using other nano- and microfabrication methods, such as irreversible chemical etching and self-assembly. Fig. 11b shows the low-magnification view; Fig. 11c, d show high-magnification views in the directions opposite to a single micropillar (viewing directions are marked in Fig. 11b). The benefits of this technique are further demonstrated by preparing a multiplexing structure-color filter with 2D metasurfaces of different periodicities (*i.e.*, different grating colors) in a compact micropillar array (Figs. 11e−k). Reflected structural colors offer significant advantages over conventional pigment-based color filters in terms of brightness, robustness, and environmental friendliness[92]. However, the integration of diverse color filters with discrete wavelength selectivities in a single compact device is complex when traditional fabrication methods are used. This is demonstrated by performing 3D photoengraving of secondary line patterns with different periodicities (*D* = 588, 686, and 833 nm) on three facets of an inverse pyramid, followed by physical vapor deposition (PVD) of a 10-nm-thick surface layer of copper to enhance the reflectivity (Fig. 11e, f). The engraved specimen is illuminated with oblique white light at an incident angle of 54.7° to the target surface and normal to the engravings, leading to the appearance of vivid structural colors, namely red, green, and blue, at individual facets of the inverse pyramids (Fig. 11k). This multiplexing structured color filter with pixelated diffraction colors integrated into a single composite color offers application potential for structure-color displays, light-tracking sensors, high-capacity optical data storage, and secure product labeling.
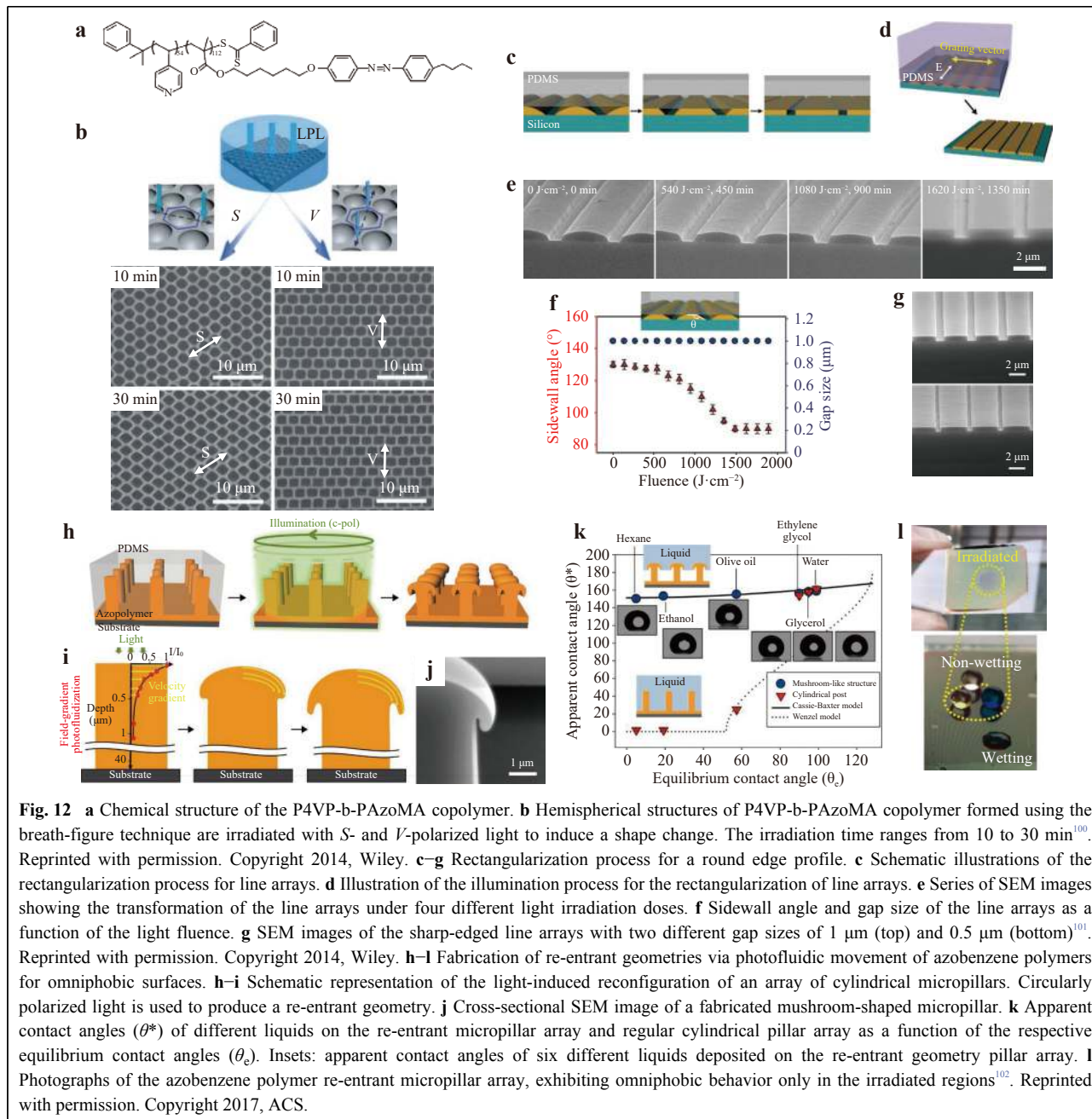
Photo-driven reconfiguration of pre-patterned structures

Isolated azobenzene polymer structures can be subjected to deterministic reshaping of the original micro- and nanostructural features (e.g., size, shape, and geometry) via single-light irradiation[23,93−96]. As discussed previously, the movement of azobenzene polymers is polarization-dependent (Fig. 4). Thus, the type of light polarization, polarization direction, or irradiation period can be adjusted to precisely reshape the pristine pattern of the azobenzene polymer, which is typically fabricated via various top-down and bottom-up methods, to form more intricate architectures[22,97−99].

For example, a hexagonal array of a hemispherical pattern of (poly(4-vinylpyridine)-*b*-poly(6-[4-(4-butyloxyphenylazo)phenoxy]hexylmethacrylate) (P4VP-b-PAzoMA) copolymer (Fig. 12a) is manufactured using the breath-figure technique, and it can be reconfigured into different patterns using single-light irradiation[100]. The polarization direction of a single laser beam, whether *S*- or *V*-polarized (see definition in Fig. 12b) determines whether the hemispheres change into rhombus-shaped structures or rectangles, whereas the duration of light irradiation controls the size of the structures. This study demonstrated the simplicity and versatility of light-based manufacturing of azobenzene polymers to reconfigure spherical patterns obtained by the bottom-up approach into arbitrary shapes.

All of the reconfigured structures after photo-driven reconfiguration of the azobenzene polymer exhibit a parabolic or round wall owing to the tendency of the photofluidized azobenzene polymer to minimize the surface area. This inherent tendency limits its use as a reconfigurable etching mask for the lithography process. To solve this problem, Kim et al. suggested a rectangularization method to render the round walls into rectangular walls[101] when the reconfigured azobenzene polymer arrays were brought into contact with a flat PDMS. Owing to the elastomeric nature of PDMS, a uniform conformal contact between the arrays and the PDMS film could be obtained. Subsequently, the azobenzene polymers were irradiated through the transparent PDMS overlay, during which the azobenzene polymers behaved as a viscoelastic fluid and adhered to the PDMS surface, resulting in a gradual rectangularization of the round wall, as shown in Fig. 12c. For a line pattern, a polarized light normal to the grating vector (Fig. 12d) was irradiated, and the irradiated azobenzene polymers flowed along the direction parallel to the light polarization but remained as a solid in other directions. Owing to the intermolecular force between the fluidized azopolymers and PDMS, an interface between the azobenzene polymers and PDMS was created to dissipate the internal stress, transforming the round edge to a rectangular edge with an increase in the light irradiation dose. The structural evolution during the rectangularization process is shown in Fig. 12e. Notably, during the early stage of irradiation, only the middle-top portion of the rounded strip in direct contact with the PDMS is flattened, whereas the sidewall angle remains unchanged, as indicated by the red triangles in Fig. 12f. As the light irradiation dose increases, the sidewall angle begins to decrease gradually with the gradual flattening of the top surface and eventually reaches 90° (i.e., with sharp edges). During the reduction of the sidewall angle, the gap size remains unchanged, as shown by the blue circles in Fig. 12f, because the light polarization is perpendicular to the grating vector. As

Fig. 12 a Chemical structure of the P4VP-b-PAzoMA copolymer. **b** Hemispherical structures of P4VP-b-PAzoMA copolymer formed using the breath-figure technique are irradiated with *S*- and *V*-polarized light to induce a shape change. The irradiation time ranges from 10 to 30 min[100]. Reprinted with permission. Copyright 2014, Wiley. **c−g** Rectangularization process for a round edge profile. **c** Schematic illustrations of the rectangularization process for line arrays. **d** Illustration of the illumination process for the rectangularization of line arrays. **e** Series of SEM images showing the transformation of the line arrays under four different light irradiation doses. **f** Sidewall angle and gap size of the line arrays as a function of the light fluence. **g** SEM images of the sharp-edged line arrays with two different gap sizes of 1 μm (top) and 0.5 μm (bottom)[101]. Reprinted with permission. Copyright 2014, Wiley. **h−l** Fabrication of re-entrant geometries via photofluidic movement of azobenzene polymers for omniphobic surfaces. **h−i** Schematic representation of the light-induced reconfiguration of an array of cylindrical micropillars. Circularly polarized light is used to produce a re-entrant geometry. **j** Cross-sectional SEM image of a fabricated mushroom-shaped micropillar. **k** Apparent contact angles (θ^*) of different liquids on the re-entrant micropillar array and regular cylindrical pillar array as a function of the respective equilibrium contact angles (θ_e). Insets: apparent contact angles of six different liquids deposited on the re-entrant geometry pillar array. **l** Photographs of the azobenzene polymer re-entrant micropillar array, exhibiting omniphobic behavior only in the irradiated regions[102]. Reprinted with permission. Copyright 2017, ACS.

shown in Fig. 12g, line patterns with a rectangular wall and different gap sizes (1 and 0.5 μm) can be successfully obtained using the rectangularization process.

A light-induced reconfiguration strategy can also be effectively used to achieve an excellent liquid-repellent surface. As shown in Figs. 12h−l, the 3D architecture of the microstructures can be designed to sustain a strong repellence to the wetting of almost any liquid, a property commonly referred to as omniphobicity, which is relevant for applications that require liquid-repellency and self-cleaning[102]. The realization of such omniphobic surfaces

typically requires the fabrication of a specific and highly engineered re-entrant geometry[103,104], which involves multi-step lithographic processes that are time-consuming, low-yield, and expensive. However, the realization of such surfaces can be made considerably easier and more cost-effective with the use of a single-step light-induced reconfiguration of an array of cylindrical microposts irradiated with circularly polarized light, as shown in Figs. 12h−j. The resulting structure can repel different types of liquids, including water, glycerol, olive oil, and ethanol (see Fig. 12k, l).

Light-driven self-healing and pore size control for water/oil separation

Polymers with azobenzene-type chromophores on the side chains, referred to as P1, have been shown to exhibit light-enabled self-healing (Fig. 13a, b)[105]. *Trans*-P1 (T_g = 48 °C) is a solid at room temperature, whereas *cis*-P1 (T_g = −10 °C) is a liquid at room temperature. Therefore, P1 undergoes reversible solid-to-liquid transitions under alternating UV and visible light irradiation at local regions. The capillary flow of the liquefied *cis*-P1 enables the repair of damage to the hard coating, and thus scratches on the P1 film are repeatedly healed. Along the line, the surface roughness of the patterns is effectively reduced during the reversible solid-to-liquid transitions.

Azobenzene polymers can also be coated on a rigid plastic (e.g., PET) to repair cracks on the substrate via irradiation with polarized light (Fig. 13c, d)[24]. The azobenzene polymers move parallel to the direction of polarization, resulting in gradual self-healing of the damage (Fig. 13c). This light-assisted behavior can be extended to repair electric conductors (Fig. 13d) consisting of silver nanowires covered by an electrically conductive azobenzene polymer film. When the coated film is scratched, a short circuit is formed; thus, LEDs arranged in a 'K'-shape are dimmed. Light irradiation-induced self-healing movement in the azobenzene polymers drags the silver nanowires near the crack to reconnect, and the LEDs light up again (Fig. 13d). This self-healing of electrically conductive and flexible films has potential applications in flexible electronic devices, where simple light irradiation can fix a short circuit without the need to change the parts. This will allow for longer product lives, thereby minimizing electronic waste.

Azobenzene polymers can be electrospun into fibers with controllable fiber and pore sizes. Membranes with hierarchical architectures, where pores of different sizes are integrated in tandem, are of great interest for water/oil emulsion separation owing to their potential for achieving a high flux, high selectivity, and mechanical durability. Such hierarchical membranes can be obtained by utilizing the photofluidic movement of PDO 3, as shown in Fig. 14[25]. Here, PDO 3 is electrospun (Fig. 14a) onto an optically inactive polycaprolactone (PCL) fibrous supporting layer. Upon light irradiation, the PDO 3 fibers undergo
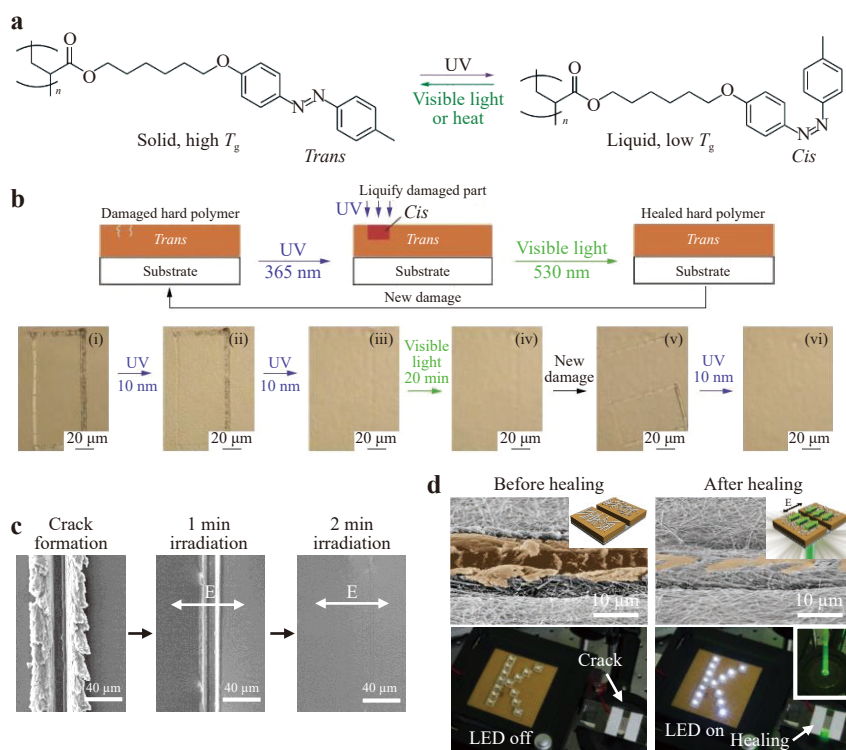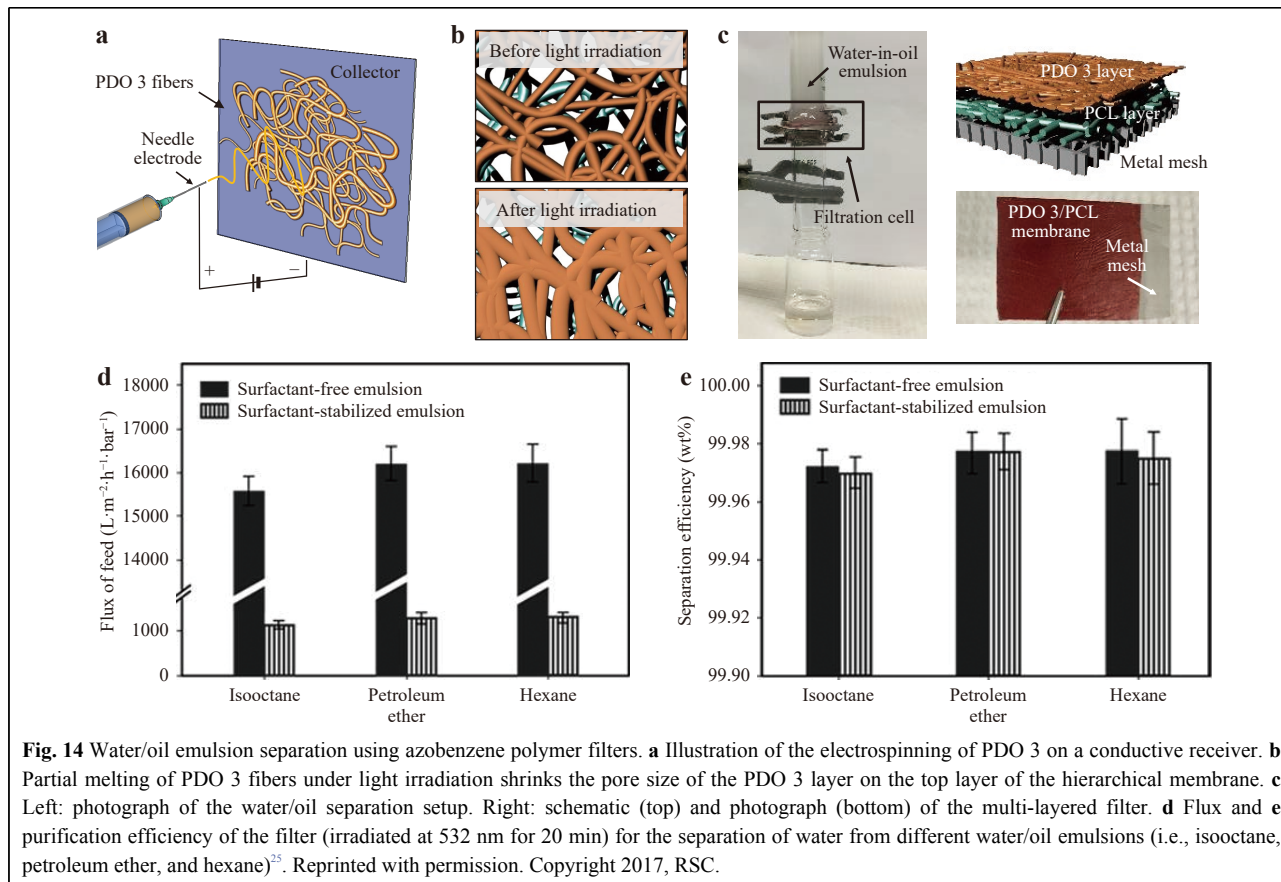

Fig. 13 a Chemical structures of *trans*-P1 and *cis*-P1. **b** Overall scheme and procedure for a light-healable azobezene polymer (P1) film. (i-vi) The damaged area on the P1 film is repeatedly healed with light irradiation[105]. Reprinted with permission. Copyright 2017, Springer Nature. **c** SEM images of the self-healing process of a crack on a PDO 3 film irradiated with light for different durations. **d** Application of an azobenzene polymer to a self-healing electrically conductive circuit. Silver nanowires are reconnected by the healing movement of the azobezene polymer to operate the LEDs[24]. Reprinted with permission. Copyright 2014, Wiley.

Fig. 14 Water/oil emulsion separation using azobenzene polymer filters. **a** Illustration of the electrospinning of PDO 3 on a conductive receiver. **b** Partial melting of PDO 3 fibers under light irradiation shrinks the pore size of the PDO 3 layer on the top layer of the hierarchical membrane. **c** Left: photograph of the water/oil separation setup. Right: schematic (top) and photograph (bottom) of the multi-layered filter. **d** Flux and **e** purification efficiency of the filter (irradiated at 532 nm for 20 min) for the separation of water from different water/oil emulsions (i.e., isooctane, petroleum ether, and hexane)[25]. Reprinted with permission. Copyright 2017, RSC.

polarization-dependent mass transport due to the photofluidization effect despite the fact that PDO 3 has a T_g of 120 °C. The electrospun PDO 3 fibrous layer partially melts, thus shrinking the pore size, while the PCL supporting layer remains intact, forming a hierarchical membrane with modified nanopores in the PDO 3 layer and micropores in the PCL layer. (Fig. 14b) The membrane performance is evaluated based on the separation of oil/water emulsions (see the experimental apparatus and procedure in Fig. 14c). The results show that the fabricated hierarchical membranes can selectively and effectively separate (> 99.96%) various droplets from both surfactant-free and surfactant-stabilized water-in-oil emulsions (sizes as small as 50 nm) solely driven by gravity with a high flux (*ca.* 15,000 L m^{-2} h^{-1} bar^{-1} for surfactant-free emulsions and *ca.* 1 000 L m^{-2} h^{-1} bar^{-1} for surfactant-stabilized emulsions) (Fig. 14d, e).

Conclusions

Herein, we briefly review the origin of the unique photofluidic movement of azobenzene polymers and their applications. The photofluidization of azobenzene groups occurs below T_g within localized regions subjected to light irradiation and can be directed anisotropically using polarized light. The extent of photofluidic movement is dependent on the light intensity and exposure time, and the material immediately solidifies upon the removal of light irradiation. Therefore, directional and temporal control of the fluidization behavior can provide a new route for manufacturing complex micro- and nanostructures over a large area in a high-throughput fashion. Moreover, the unusual photofluidic movement can be effectively employed in many applications, including light-enabled reconfiguration of flat and pre-patterned surfaces for wettability, adhesion, photonics, and lithography; self-healing of electrical circuits; and filters for oil/water separation. New applications may emerge in the future with the design and adoption of novel molecular strategies for efficient and large surface modulation, complex light illumination, suitable pre-structuration, and utilization of the reversible nature of the phenomena involved. Elucidating the exact mechanism of the unusual photofluidic movement is a prerequisite for exploring further applications. The light-driven motion of the isomerization of azobenzene molecules and macroscopic mass transport remain to be elucidated in the context of

fundamental light–matter interactions. For practical applications, the process stability, balance of costs, and possible areas of patterns, which are closely related to the light irradiation process during photofluidic movement, are critical obstacles to overcome.

Conflict of interest
The authors declare that they have no conflict of interest.

References

1. Feng, J. et al. Light manipulation in organic light-emitting devices by integrating micro/nano patterns. *Laser & Photonics Reviews* **11**, 1600145 (2017).
2. Kim, D. H. et al. Biomimetic nanopatterns as enabling tools for analysis and control of live cells. *Advanced Materials* **22**, 4551-4566 (2010).
3. Shin, D. O. et al. Multicomponent nanopatterns by directed block copolymer self-assembly. *ACS Nano* **7**, 8899-8907 (2013).
4. Del Barrio, J. & Sánchez-Somolinos, C. Light to shape the future: from photolithography to 4D printing. *Advanced Optical Materials* **7**, 1900598 (2019).
5. Zhang, C. et al. Review of imprinted polymer microrings as ultrasound detectors: design, fabrication, and characterization. *IEEE Sensors Journal* **15**, 3241-3248 (2015).
6. Fan, H. J., Werner, P. & Zacharias, M. Semiconductor nanowires: from self-organization to patterned growth. *Small* **2**, 700-717 (2006).
7. Kim, S. O. et al. Epitaxial self-assembly of block copolymers on lithographically defined nanopatterned substrates. *Nature* **424**, 411-414 (2003).
8. Habault, D., Zhang, H. J. & Zhao, Y. Light-triggered self-healing and shape-memory polymers. *Chemical Society Reviews* **42**, 7244-7256 (2013).
9. Wang, D. R. & Wang, X. G. Amphiphilic azo polymers: molecular engineering, self-assembly and photoresponsive properties. *Progress in Polymer Science* **38**, 271-301 (2013).
10. Wang, Y. P. et al. Block copolymer aggregates with photo-responsive switches: towards a controllable supramolecular container. *Polymer* **50**, 4821-4828 (2009).
11. Natansohn, A. & Rochon, P. Photoinduced motions in azo-containing polymers. *Chemical Reviews* **102**, 4139-4176 (2002).
12. Itoga, K. et al. Cell micropatterning using photopolymerization with a liquid crystal device commercial projector. *Biomaterials* **25**, 2047-2053 (2004).
13. Rayner, D. M., Naumov, A. & Corkum, P. B. Ultrashort pulse non-linear optical absorption in transparent media. *Optics Express* **13**, 3208-3217 (2005).
14. Yesodha, S. K., Pillai, C. K. S. & Tsutsumi, N. Stable polymeric materials for nonlinear optics: a review based on azobenzene systems. *Progress in Polymer Science* **29**, 45-74 (2004).
15. Choi, B. Y. et al. Conformational molecular switch of the azobenzene molecule: a scanning tunneling microscopy study. *Physical Review Letters* **96**, 156106 (2006).
16. Zhu, L. L. et al. Luminescent color conversion on cyanostilbene-functionalized quantum dots via in-situ photo-tuning. *Advanced Materials* **24**, 4020-4024 (2012).
17. Byrne, R. et al. Characterisation and analytical potential of a photo-responsive polymeric material based on spiropyran. *Biosensors and Bioelectronics* **26**, 1392-1398 (2010).
18. Berkovic, G., Krongauz, V. & Weiss, V. Spiropyrans and spirooxazines for memories and switches. *Chemical Reviews* **100**, 1741-1754 (2000).
19. Yokoyama, Y. Fulgides for memories and switches. *Chemical Reviews* **100**, 1717-1740 (2000).
20. Pang, X. L. et al. Photodeformable azobenzene-containing liquid crystal polymers and soft actuators. *Advanced Materials* **31**, 1904224 (2019).
21. Karageorgiev, P. et al. From anisotropic photo-fluidity towards nanomanipulation in the optical near-field. *Nature Materials* **4**, 699-703 (2005).
22. Probst, C. et al. Athermal azobenzene-based nanoimprint lithography. *Advanced Materials* **28**, 2624-2628 (2016).
23. Priimagi, A. & Shevchenko, A. Azopolymer-based micro-and nanopatterning for photonic applications. *Journal of Polymer Science Part B:Polymer Physics* **52**, 163-182 (2014).
24. Kang, H. S. et al. Light-powered healing of a wearable electrical conductor. *Advanced Functional Materials* **24**, 7273-7283 (2014).
25. Kang, H. S. et al. Hierarchical membranes with size-controlled nanopores from photofluidization of electrospun azobenzene polymer fibers. *Journal of Materials Chemistry A* **5**, 18762-18769 (2017).
26. Merino, E. & Ribagorda, M. Control over molecular motion using the *cis–trans* photoisomerization of the azo group. *Beilstein Journal of Organic Chemistry* **8**, 1071-1090 (2012).
27. Goulet-Hanssens, A. et al. Electrocatalytic $Z \rightarrow E$ isomerization of azobenzenes. *Journal of the American Chemical Society* **139**, 335-341 (2017).
28. Yu, H. F. Photoresponsive liquid crystalline block copolymers: from photonics to nanotechnology. *Progress in Polymer Science* **39**, 781-815 (2014).
29. Mavrona, E. et al. Intrinsic and photo-induced properties of high refractive index azobenzene based thin films. *Optical Materials Express* **8**, 420-430 (2018).
30. Hartley, G. S. The cis-form of azobenzene. *Nature* **140**, 281 (1937).
31. Chang, J. B. et al. Effect of dye structure on orientational behavior and transition dipole moments in coatable guest–host polarizers. *Dyes and Pigments* **121**, 30-37 (2015).
32. Barrett, C. J. et al. Photo-mechanical effects in azobenzene-containing soft materials. *Soft Matter* **3**, 1249-1261 (2007).
33. Akiyama, H. & Yoshida, M. Photochemically reversible liquefaction and solidification of single compounds based on a sugar alcohol scaffold with multi azo-arms. *Advanced Materials* **24**, 2353-2356 (2012).
34. Yager, K. G. & Barrett, C. J. Temperature modeling of laser-irradiated azo-polymer thin films. *The Journal of Chemical Physics* **120**, 1089-1096 (2004).
35. Barrett, C. J., Natansohn, A. L. & Rochon, P. L. Mechanism of optically inscribed high-efficiency diffraction gratings in azo polymer films. *The Journal of Physical Chemistry* **100**, 8836-8842 (1996).
36. Pedersen, T. G. et al. Mean-field theory of photoinduced formation of surface reliefs in side-chain azobenzene polymers. *Physical Review Letters* **80**, 89-92 (1998).
37. Kumar, J. et al. Gradient force: the mechanism for surface relief

grating formation in azobenzene functionalized polymers. *Applied Physics Letters* **72**, 2096-2098 (1998).

38. Bian, S. P. et al. Photoinduced surface relief grating on amorphous poly (4-phenylazophenol) films. *Chemistry of Materials* **12**, 1585-1590 (2000).

39. Lefin, P., Fiorini, C. & Nunzi, J. M. Anisotropy of the photo-induced translation diffusion of azobenzene dyes in polymer matrices. *Pure and Applied Optics:Journal of the European Optical Society Part A* **7**, 71-82 (1998).

40. Juan, M. L. et al. Multiscale model for photoinduced molecular motion in azo polymers. *ACS Nano* **3**, 1573-1579 (2009).

41. Lednev, I. K. et al. Femtosecond time-resolved UV-visible absorption spectroscopy of trans-azobenzene: dependence on excitation wavelength. *Chemical Physics Letters* **290**, 68-74 (1998).

42. Kang, H. S. et al. Multi-level micro/nanotexturing by three-dimensionally controlled photofluidization and its use in plasmonic applications. *Advanced Materials* **25**, 5490-5497 (2013).

43. Fang, G. J. et al. Athermal photofluidization of glasses. *Nature Communications* **4**, 1521 (2013).

44. Xie, S., Natansohn, A. & Rochon, P. Microstructure of copolymers containing Disperse Red 1 and methyl methacrylate. *Macromolecules* **27**, 1885-1890 (1994).

45. Viswanathan, N. K. et al. Surface relief structures on azo polymer films. *Journal of Materials Chemistry* **9**, 1941-1955 (1999).

46. Ambrosio, A. et al. Light-induced spiral mass transport in azo-polymer films under vortex-beam illumination. *Nature Communications* **3**, 989 (2012).

47. Hubert, C. et al. Spontaneous patterning of hexagonal structures in an azo-polymer using light-controlled mass transport. *Advanced Materials* **14**, 729-732 (2002).

48. Zhou, X. R., Du, Y. & Wang, X. G. Azo polymer janus particles and their photoinduced, symmetry-breaking deformation. *ACS Macro Letters* **5**, 234-237 (2016).

49. Lee, S. H. et al. Azo polymer multilayer films by electrostatic self-assembly and layer-by-layer post azo functionalization. *Macromolecules* **33**, 6534-6540 (2000).

50. Ambrosio, A., Maddalena, P. & Marrucci, L. Molecular model for light-driven spiral mass transport in azopolymer films. *Physical Review Letters* **110**, 146102 (2013).

51. Kang, H. S., Lee, S. & Park, J. K. Monolithic, hierarchical surface reliefs by holographic photofluidization of azopolymer arrays: direct visualization of polymeric flows. *Advanced Functional Materials* **21**, 4412-4422 (2011).

52. Wang, X. L., Yin, J. J. & Wang, X. G. Photoinduced self-structured surface pattern on a molecular azo glass film: structure–property relationship and wavelength correlation. *Langmuir* **27**, 12666-12676 (2011).

53. Kang, H. S. et al. Light-induced surface patterning of silica. *ACS Nano* **9**, 9837-9848 (2015).

54. Koskela, J. E. et al. Light-fuelled transport of large dendrimers and proteins. *Journal of the American Chemical Society* **136**, 6850-6853 (2014).

55. Ubukata, T., Isoshima, T. & Hara, M. Wavelength-programmable organic distributed-feedback laser based on a photoassisted polymer-migration system. *Advanced Materials* **17**, 1630-1633 (2005).

56. Yadavalli, N. S. et al. Structuring of photosensitive material below diffraction limit using far field irradiation. *Applied Physics A* **113**, 263-272 (2013).

57. Jelken, J., Henkel, C. & Santer, S. Formation of half-period surface relief gratings in azobenzene containing polymer films. *Applied Physics B* **126**, 149 (2020).

58. Emoto, A., Uchida, E. & Fukuda, T. Optical and physical applications of photocontrollable materials: azobenzene-containing and liquid crystalline polymers. *Polymers* **4**, 150-186 (2012).

59. Kang, H. S. et al. Three-dimensional photoengraving of monolithic, multifaceted metasurfaces. *Advanced Materials* **33**, 2005454 (2020).

60. Oscurato, S. L. et al. From nanoscopic to macroscopic photo-driven motion in azobenzene-containing materials. *Nanophotonics* **7**, 1387-1422 (2018).

61. Salvatore, M., Borbone, F. & Oscurato, S. L. Deterministic realization of quasicrystal surface relief gratings on thin azopolymer films. *Advanced Materials Interfaces* **7**, 1902118 (2020).

62. Sakhno, O. et al. Deep surface relief grating in azobenzene-containing materials using a low-intensity 532 nm laser. *Optical Materials:X* **1**, 100006 (2019).

63. Samanta, D. et al. Reversible photoswitching of encapsulated azobenzenes in water. *Proceedings of the National Academy of Sciences of the United States of America* **115**, 9379-9384 (2018).

64. Shirazi, H. D. et al. Multiscale hierarchical surface patterns by coupling optical patterning and thermal shrinkage. *ACS Applied Materials & Interfaces* **13**, 15563-15571 (2021).

65. Kravchenko, A. et al. Optical interference lithography using azobenzene-functionalized polymers for micro-and nanopatterning of silicon. *Advanced Materials* **23**, 4174-4177 (2011).

66. Ambrosio, A. et al. Controlling spontaneous surface structuring of azobenzene-containing polymers for large-scale nano-lithography of functional substrates. *Applied Physics Letters* **102**, 093102 (2013).

67. Hendrikx, M. et al. Light-triggered formation of surface topographies in azo polymers. *Crystals* **7**, 231 (2017).

68. Labarthet, F. L., Buffeteau, T. & Sourisseau, C. Azopolymer holographic diffraction gratings: time dependent analyses of the diffraction efficiency, birefringence, and surface modulation induced by two linearly polarized interfering beams. *The Journal of Physical Chemistry B* **103**, 6690-6699 (1999).

69. Xiong, Z. Y., Liao, C. L. & Wang, X. G. Reduced graphene oxide diffraction gratings from duplication of photoinduced azo polymer surface-relief-gratings through soft-lithography. *Journal of Materials Chemistry C* **3**, 6224-6231 (2015).

70. Labarthet, F. L., Buffeteau, T. & Sourisseau, C. Analyses of the diffraction efficiencies, birefringence, and surface relief gratings on azobenzene-containing polymer films. *Journal of Physical Chemistry B* **102**, 2654-2662 (1998).

71. Lee, S., Jeong, Y. C. & Park, J. K. Facile fabrication of close-packed microlens arrays using photoinduced surface relief structures as templates. *Optics Express* **15**, 14550-14559 (2007).

72. Hong, J. C. et al. Photoinduced tuning of optical stop bands in azopolymer based inverse opal photonic crystals. *Advanced Functional Materials* **17**, 2462-2469 (2007).

73. Kossifos, K. M. et al. An optically-programmable absorbing metasurface. Proceedings of the 2018 IEEE International Symposium on Circuits and Systems (ISCAS). Florence: IEEE, 2018: 1-5.

74. Zhang, G. Q. et al. Tailoring nanohole plasmonic resonance with light-responsive azobenzene compound. *ACS Applied Materials & Interfaces* **11**, 2254-2263 (2019).

75. Choi, C. H. & Kim, C. J. Fabrication of a dense array of tall nanostructures over a large sample area with sidewall profile and tip sharpness control. *Nanotechnology* **17**, 5326-5333 (2006).

76. Wang, K. X. et al. Absorption enhancement in ultrathin crystalline silicon solar cells with antireflection and light-trapping nanocone gratings. *Nano Letters* **12**, 1616-1619 (2012).

77. Moerland, R. J. et al. Large-area arrays of three-dimensional plasmonic subwavelength-sized structures from azopolymer surface-relief gratings. *Materials Horizons* **1**, 74-80 (2014).

78. Liu, B. et al. Duplication of photoinduced azo polymer surface-relief

gratings through a soft lithographic approach. *Langmuir* **22**, 7405-7410 (2006).

79. Na, S. I. et al. Surface relief gratings on poly (3-hexylthiophene) and fullerene blends for efficient organic solar cells. *Applied Physics Letters* **91**, 173509 (2007).

80. Jeong, S. M. et al. Enhancement of light extraction from organic light-emitting diodes with two-dimensional hexagonally nanoimprinted periodic structures using sequential surface relief grating. *Japanese Journal of Applied Physics* **47**, 4566-4571 (2008).

81. Paterson, J. et al. Optically inscribed surface relief diffraction gratings on azobenzene-containing polymers for coupling light into slab waveguides. *Applied Physics Letters* **69**, 3318-3320 (1996).

82. Madani, A. et al. Experimental study of liquid-crystal alignment on a surface relief grating. *Laser Physics* **16**, 1197-1201 (2006).

83. Zhao, Y. et al. Anisotropic wetting characteristics on submicrometer-scale periodic grooved surface. *Langmuir* **23**, 6212-6217 (2007).

84. Wu, D. et al. A simple strategy to realize biomimetic surfaces with controlled anisotropic wetting. *Applied Physics Letters* **96**, 053704 (2010).

85. Xia, D. Y., Johnson, L. M. & López, G. P. Anisotropic wetting surfaces with one-dimesional and directional structures: fabrication approaches, wetting properties and potential applications. *Advanced Materials* **24**, 1287-1302 (2012).

86. Oscurato, S. L. et al. Light-driven wettability tailoring of azopolymer surfaces with reconfigured three-dimensional posts. *ACS Applied Materials & Interfaces* **9**, 30133-30142 (2017).

87. Wu, H. et al. Large area metal micro-/nano-groove arrays with both structural color and anisotropic wetting fabricated by one-step focused laser interference lithography. *Nanoscale* **11**, 4803-4810 (2019).

88. Jiang, S. J. et al. Multifunctional Janus microplates arrays actuated by magnetic fields for water/light switches and bio-inspired assimilatory coloration. *Advanced Materials* **31**, 1807507 (2019).

89. Kusumaatmaja, H. et al. Anisotropic drop morphologies on corrugated surfaces. *Langmuir* **24**, 7299-7308 (2008).

90. Rianna, C. et al. Reversible holographic patterns on azopolymers for guiding cell adhesion and orientation. *ACS Applied Materials & Interfaces* **7**, 16984-16991 (2015).

91. Cabezas, M. D. et al. Subcellular control over focal adhesion anisotropy, independent of cell morphology, dictates stem cell fate. *ACS Nano* **13**, 11144-11152 (2019).

92. Zhao, Y. J. et al. Bio-inspired variable structural color materials. *Chemical Society Reviews* **41**, 3297-3317 (2012).

93. Lee, S., Kang, H. S. & Park, J. K. Directional photofluidization lithography: micro/nanostructural evolution by photofluidic motions of azobenzene materials. *Advanced Materials* **24**, 2069-2103 (2012).

94. Wang, W. et al. Deterministic reshaping of breath figure arrays by directional photomanipulation. *ACS Applied Materials & Interfaces* **9**, 4223-4230 (2017).

95. Wang, W. et al. Directional photo-manipulation of self-assembly patterned microstructures. *Chinese Journal of Polymer Science* **36**, 297-305 (2018).

96. Kong, X. L. et al. Photomanipulated architecture and patterning of azopolymer array. *ACS Applied Materials & Interfaces* **9**, 19345-19353 (2017).

97. Li, Y. B. et al. Formation of photoresponsive uniform colloidal spheres from an amphiphilic azobenzene-containing random copolymer. *Macromolecules* **39**, 1108-1115 (2006).

98. Li, Y. B. et al. Photoinduced deformation of amphiphilic azo polymer colloidal spheres. *Journal of the American Chemical Society* **127**, 2402-2403 (2005).

99. Yang, B. W., Yu, M. M. & Yu, H. F. Azopolymer-based nanoimprint lithography: recent developments in methodology and applications. *ChemPlusChem* **85**, 2166-2176 (2020).

100. Wang, W. et al. Directional photomanipulation of breath figure arrays. *Angewandte Chemie International Edition* **53**, 12116-12119 (2014).

101. Choi, J. et al. Photo-reconfigurable azopolymer etch mask: photofluidization-driven reconfiguration and edge rectangularization. *Small* **14**, 1703250 (2018).

102. Choi, J. et al. Flexible and robust superomniphobic surfaces created by localized photofluidization of azopolymer pillars. *ACS Nano* **11**, 7821-7828 (2017).

103. Wu, Y. et al. Bioinspired design of three-dimensional ordered tribrachia-post arrays with re-entrant geometry for omniphobic and slippery surfaces. *ACS Nano* **11**, 8265-8272 (2017).

104. Utech, S. et al. Tailoring re-entrant geometry in inverse colloidal monolayers to control surface wettability. *Journal of Materials Chemistry A* **4**, 6853-6859 (2016).

105. Zhou, H. W. et al. Photoswitching of glass transition temperatures of azobenzene-containing polymers induces reversible solid-to-liquid transitions. *Nature Chemistry* **9**, 145-151 (2017).